

## Magnetic neutron scattering in dilute AlMn alloy

N. Kroó

Central Research Institute for Physics, Budapest, Hungary

Z. Szentirmay\*

Joint Institute for Nuclear Research, Dubna, USSR

(Received 27 June 1973)

Neutron scattering studies were performed on an Al-0.5-at.-%-Mn dilute alloy at  $T = 80^\circ\text{K}$  and  $T = 300^\circ\text{K}$  sample temperatures. The incoherent magnetic scattering cross section was measured using the Dubna pulsed reactor as a function of in-going neutron energy, at four scattering angles. The results show a nonzero magnetic moment on the Mn sites and a  $\xi \sim 6\text{-\AA}$  radius oppositely polarized electron cloud around these atoms.

### I. INTRODUCTION

If the lattice of a nonmagnetic matrix metal contains a small number of magnetic atoms in statistical distribution, incoherent magnetic scattering of thermal neutrons will occur, the energy and angular distribution of which are characteristic of the time and space dependence of the perturbation. This enables immediate investigation of localized magnetic moments and may help to answer some fundamental questions concerning dilute magnetic alloys. The fundamental theories of dilute magnetic alloys are based on the so-called *s-d-exchange* and *localized-spin-fluctuation* (LSF) models.

In the *s-d-exchange* model the system is taken to be essentially magnetic. The magnetic moments localized on impurities are in static or dynamic interaction with the surrounding conduction-electron cloud, which is polarized in the opposite direction to the localized moment. This compensating cloud is definitely not larger than  $10\text{ \AA}$  in diameter, so that the scattering intensity is likely to be proportional to the effective form factor of the cloud plus impurity for small scattering vectors, and to the paramagnetic form factor of the localized moment for  $\kappa > 1\text{ \AA}^{-1}$ .

According to the LSF model, in contrast, there is no compensating cloud. The system is essentially nonmagnetic, and its properties are determined by so-called localized spin fluctuations with a finite relaxation time. Since, however, the relation of the LSF model to neutron scattering has not yet been elaborated we shall use here, as our working hypothesis, the theory based on the *s-d-exchange* model.

The ground state of dilute magnetic alloys has been studied by Gurgenshili, Nersesian, and Haradze<sup>1</sup> starting from a dynamic interpretation of the *s-d-exchange* model. They assume that an impurity atom preserves its magnetic moment in the alloy but it enters into dynamic interaction with the surrounding polarized electron cloud at

low temperatures. The spectral density function  $S(\omega)$  of the localized spin fluctuations has a maximum at  $\omega \sim k_B T_K$ , while it tends to zero for  $\omega \rightarrow 0$ , if  $T \rightarrow 0$ , as shown in Fig. 1. The halfwidth of  $S(\omega)$  is in the order of  $k_B T_K$ . The cross section for magnetic neutron scattering calculated on the basis of this theory indicates that the incoherent paramagnetic scattering is perfectly inelastic at  $T \sim 0$  and can be characterized by  $S(\omega)$  and an effective form factor  $\tilde{F}(\kappa)$ . The paramagnetic scattering in the Bragg direction, on the other hand, consists of an elastic component proportional to the effective form factor and the static susceptibility, in accordance with the measurements obtained by Stassis and Shull.<sup>2</sup>

The double differential cross section  $d^2\sigma/d\Omega dE$  for magnetic incoherent scattering is proportional to both  $S(\omega)$  and  $\tilde{F}^2(\kappa)$ . The measurement of this quantity therefore contains all the pertinent information. If, however, the neutron flux is not high

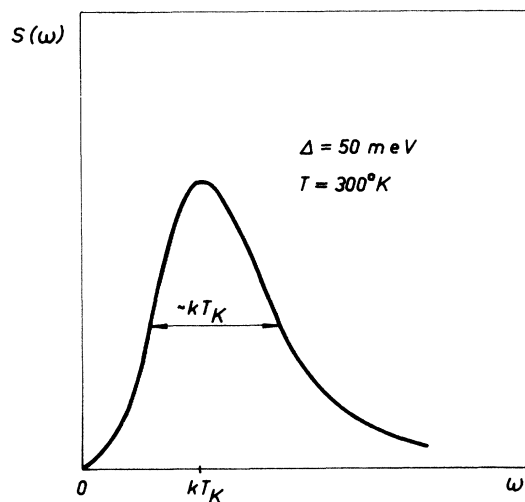


FIG. 1. Spectral density function  $S(\omega)$  of localized spin fluctuations.

enough—and this is the case with most of the present working reactors—the intensity scattered by impurity systems is too low. It was shown, by Gurgenshili and his colleagues, however, that the cross section  $d\sigma(E_0)/d\Omega = \int (d^2\sigma/d\Omega dE) dE$ , which is integrated for the final neutron energies, still shows the most important features of the system, i. e., the effect on the scattering pattern of  $S(\omega)$  and of the change in  $F(\kappa)$  due to polarization.

## II. PREPARATION OF THE SAMPLES

Our experiments were carried out on the Al-0.5-at.-%-Mn system.<sup>3</sup> Aluminum as a matrix metal has an incoherent scattering cross section of practically zero and can therefore be favorably used for neutron physical measurements; furthermore AlMn dilute alloy has a Kondo temperature high enough to enable investigation of the ground state even at room temperature ( $T_K = 450\text{--}1200^\circ\text{K}$ , according to different measurements).

The polycrystalline samples were made of 99.995%-pure Al containing 50-ppm iron and alloyed with 0.5-at.-% Mn. The 2-mm-thick and 20-mm-wide layers rolled from this alloy were quenched in water after a 10-h period of homogenizing annealing at  $630^\circ\text{C}$ . No precipitation could be detected on optical examination of the samples; the crystallites had an average diameter of 0.6 mm. The Mn concentration was determined by the standard method of permanganometry.

Sheets containing no Mn were also prepared from the same matrix material. Since cold rolling of Al sheets results in a wide variation in grain size, experiments were carried out on samples where the average grain size was altered by heat treatment to the 0.3–0.9-mm range. Neutron scattering patterns did not change in the  $E_0, \kappa$  region examined for samples with different grain sizes. The Al and AlMn sheets were stacked into  $12 \times 80 \times 100$ -mm packets interleaved with Cd absorbers arranged perpendicular to the sample plane in order to reduce multiple scattering. The thickness of the irradiated samples was constant

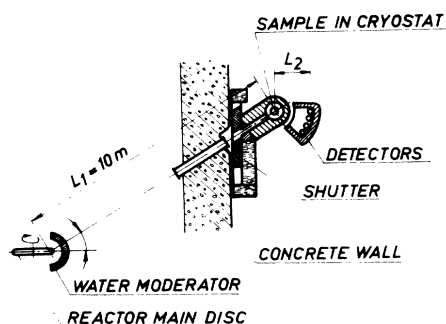


FIG. 2. Experimental arrangement for the measurement of  $d\sigma(E_0)/d\Omega$  using the IBR-30 reactor.

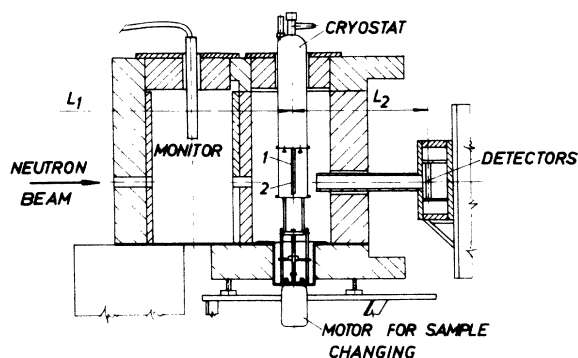


FIG. 3. Cryostat containing samples 1 and 2, showing sample changing device, detectors, and shielding.

within 0.5%.

## III. EXPERIMENTS

The scattering intensities of neutrons of 20–300-meV bombarding energy on the samples are measured at  $T = 80$  and  $300^\circ\text{K}$  using the IBR-30 fast pulsed reactor in Dubna. The experimental arrangement is shown in Fig. 2. The pulse frequency was 100 Hz, pulse length 2–3  $\mu\text{sec}$ , average thermal power of the reactor 6 kW, and maximum power in a pulse about 30 MW.

The aim was to measure the cross section of diffuse magnetic scattering  $[d\sigma(E_0)/d\Omega]_M$  as a function of the in-going neutron energy. For  $T < T_K$  this scattering is almost perfectly inelastic according to.<sup>1</sup> Since only a very small effect was expected due to the low impurity concentration, the sample-to-moderator and sample-to-detector distances,  $L_1$  and  $L_2$ , were chosen so that  $L_2/L_1 \ll 1$ . Thus, when using the time-of-flight technique, neutrons scattered from the sample both elastically and inelastically are detected at practically the same instant, which means that the entire spectrum of the thermal neutron beam can be utilized and the measured quantity will in fact be the cross section  $d\sigma(E_0)/d\Omega$ . The holder containing the Al-0.5-at.-%-Mn and pure-Al samples, one under the other, was placed in a cryostat (Fig. 3). The measurements were performed in 5-min cycles with the help of an automatic sample changer controlled by a monitor counter. Halfway through the measurements, the two samples were interchanged in order to avoid geometric errors.

Scattered neutrons were detected with four  $\text{BF}_3$  detectors positioned at angles of  $\xi = 8^\circ; 11.7^\circ; 15.4^\circ; 19.1^\circ$ . It was found that detection was not possible for  $\vartheta < 8^\circ$ , owing to the high background level, nor for  $\vartheta > 20^\circ$ , owing to Bragg reflections in the Al matrix. The intensity distribution versus flight times of the neutrons scattered on both the AlMn and the Al samples were determined with the same 4096-channel analyzer.

To standardize experimental results, a 2-mm-thick vanadium layer was used as a reference sample in the same geometrical arrangement, its spectrum being determined alternately with background measurements.

The neutron scattering intensity consists of the following components:

$$\begin{aligned}\phi(\text{Al}) &= \phi_{\text{inc}} + \phi_m + \phi_{\text{ph}} + \phi_g, \\ \phi(\text{AlMn}) &= \phi_{\text{inc}} + \phi_{\text{is,inc}} + \phi'_m + \phi'_g + \phi'_{\text{ph}} + \phi_M,\end{aligned}\quad (1)$$

where  $\phi_{\text{inc}}$ ,  $\phi_{\text{is,inc}}$ ,  $\phi_m$ , and  $\phi_M$  are the intensities of incoherent, nuclear-isotope incoherent, multiple, and paramagnetic scattering, respectively, and  $\phi_g$  and  $\phi_{\text{ph}}$  are the contributions from neutrons scattered on grain boundaries and lattice vibrations. Since Al has a relatively high Debye temperature ( $\Theta_D \approx 400^\circ\text{K}$ ) and the cross section of incoherent scattering is very small ( $\sigma_{\text{inc}} \approx 0$ ), it may be assumed that  $\phi_{\text{ph}} - \phi'_{\text{ph}} \ll \phi_M$ . This approximation would certainly not be valid if a resonant phonon mode played a role in the scattering process. Since, however, the expected broad virtual resonance  $E_r < 20$  meV and experimental data were considered in the  $E_0 > 20$ -meV range the contribution of the resonant mode to the incoherent nuclear

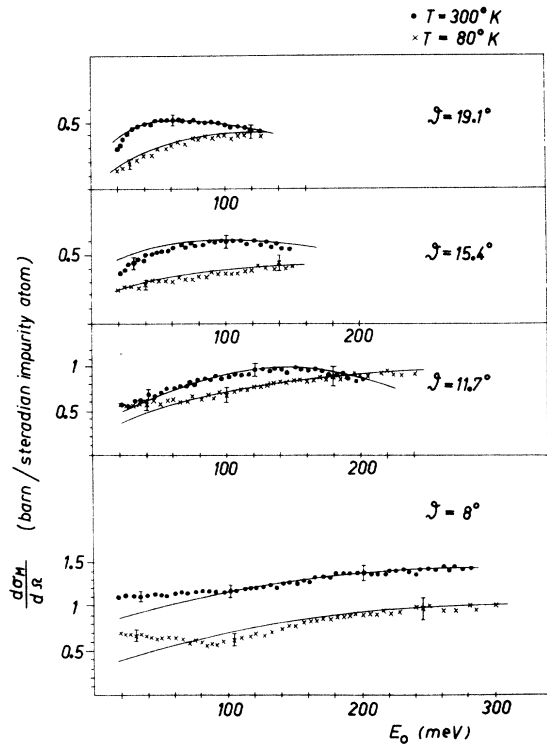


FIG. 4. Differential cross section of the paramagnetic scattering in AlMn alloy at 80 and 300°K as a function of the in-going neutron energy for different scattering angles. The solid lines are the theoretical curves normalized to the experimental results at high energies (Ref. 1).

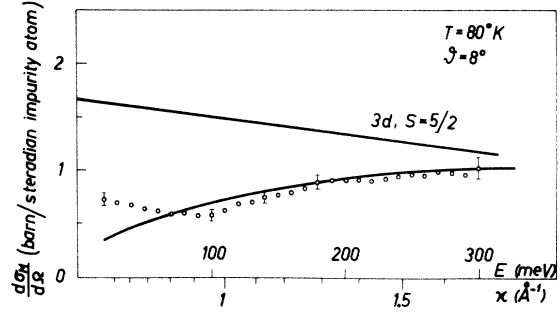


FIG. 5. Plots of  $d\sigma/d\Omega$  for  $\xi = 8^\circ$  and  $T = 80^\circ$  vs in-going neutron energy and momentum transfer  $\kappa$ . Also indicated are the values of the elastic paramagnetic scattering obtained with the form factor of an isolated Mn ion.

scattering cross section does not lead to irregularities in the studied energy range. In addition, since the nuclear incoherent cross section is smaller than the magnetic one and only a small fraction of it is connected with inelastic processes, even the monotonous contribution of the scattering by the resonant phonon mode is small. Furthermore, for  $\vartheta > 8^\circ$  and  $\lambda < 2 \text{ \AA}$  it holds that  $\phi_g \approx \phi'_g \ll \phi_M$  due to the relatively large grain size. This statement is experimentally proved by the same form of scattered spectra in the 0.3–0.9-mm average grain size range in all the  $\kappa, E$  region but at the smallest energy part of the  $\vartheta = 8^\circ$  spectrum of Fig. 4. Thus, only three correction terms need to be taken into consideration in the differential spectrum of the doped and pure Al, viz.,  $\phi_{\text{is,inc}}$ ,  $\phi'_m$ , and  $\phi_m$  the latter two being significant only if  $\kappa$  is small:

$$\begin{aligned}\frac{d\sigma}{d\Omega} &= K\Delta\phi = K[\phi(\text{AlMn}) - \phi(\text{Al})] \\ &= K[\phi_{\text{is,inc}} + \phi_M + \Delta\phi_m].\end{aligned}\quad (2)$$

The value of  $K$  was determined by normalizing the spectrum with the help of the control measurements on the vanadium reference sample.

The above relations were sufficient to determine the differential cross section of paramagnetic scattering. The  $(d\sigma/d\Omega)_M$  data, given in units of barn/steradian impurity atom, are plotted against in-going neutron energy with temperature and scattering angle as parameters in Fig. 4. Error limits of the measurement points, which were obtained by averaging over successive 5-meV intervals, were determined by means of the Gaussian error law. As seen in Fig. 5 the measured data, at the small scattering angle run lie below the cross section for the free Mn ion and have a different character.

The value of  $\sigma_{\text{is,inc}}$  is about  $6 \cdot 10^{-3}$  b/atom while

the correction term  $\Delta(d\sigma/d\Omega)_m$  becomes significant only for small momentum transfer (Fig. 5) as stated earlier.

#### IV. DISCUSSION

As mentioned in Sec. I, the magnetic-neutron-scattering cross section has already been calculated by Gurgenshivili *et al.*<sup>1</sup> on the basis of the Kondo model. We shall therefore use these values as a working hypothesis and compare the resulting theoretical formulas with our experiment. Two regions of  $\kappa$  (i. e., two regions of ingoing energy at a fixed scattering angle) are of interest:

(a) For sufficiently high  $\kappa$  values, the law of diffuse paramagnetic scattering should apply to our results

$$\frac{d\sigma_M}{d\Omega} = \frac{2}{3} N_i (\gamma r_0)^2 S(S+1) |F(\kappa)|^2, \quad (3)$$

where  $N_i$  is the number of impurity atoms in the sample,  $\gamma$  is the magnetic moment of a neutron,  $r_0$  is the classical electron radius, and  $S$  is the absolute value of the impurity spin. The experimental  $d\sigma_M/d\Omega$  data for this region, with the exception of those obtained at  $\vartheta = 8^\circ$ , where  $\kappa$  is not large enough and therefore Eq. (3) is not valid, corresponded to  $[F(\kappa)^2]$  calculated for free manganese ions (Fig. 6). A value of  $S = 1.85$  can be determined for the localized spin from the high-energy part of these curves. In Fig. 7 the differential cross section calculated from Eq. (3) with this spin value is compared with the data measured at  $\vartheta = 19.1^\circ$  and  $T = 300^\circ\text{K}$ . It is seen that these data fit the calculated curve within the experimental error if  $\kappa > 2.2 \text{ \AA}^{-1}$ .

(b) If the region of small momentum change (i. e., low in-going energy) is considered, the magnetic

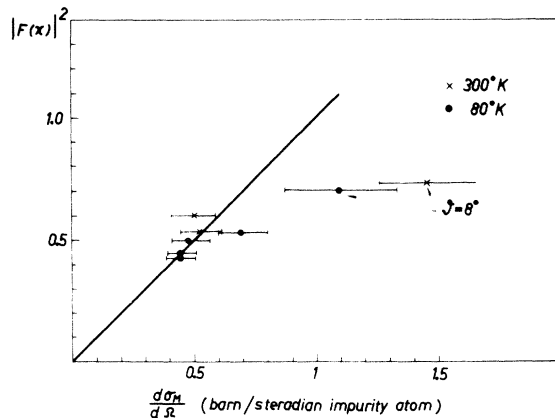


FIG. 6. Comparison of the experimental  $d\sigma_M/d\Omega$  cross section obtained for higher  $\kappa$  with the  $F^2(\kappa)$  values of free Mn ions.

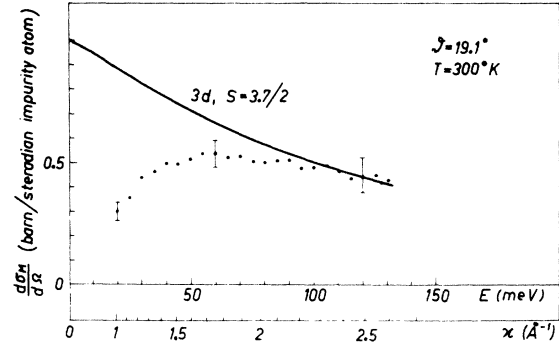


FIG. 7. Comparison of measured room-temperature data at  $\vartheta = 19.1^\circ$  with calculated elastic paramagnetic cross section.

impurity scattering is essentially characterized by the spectral density function of spin fluctuations  $S(\omega)$ ; this statement is valid if  $T \ll T_K$ .

The differential cross section  $d\sigma_M/d\Omega$  is proportional to the integral of  $S(\omega)$ . For not too low  $\kappa$  values, we have

$$\frac{d\sigma_M}{d\Omega} = \frac{2}{3} N_i (\gamma r_0)^2 \int_{-\infty}^{E_0} \left(1 - \frac{\omega}{E_0}\right)^{1/2} S(\omega) |F(\kappa)|^2 d\omega, \quad (4)$$

where  $E$  is the ingoing neutron energy and  $\omega = E_0 - E$  is the energy transfer. The density function  $S(\omega)$ , which exhibits a maximum at  $\omega \equiv \Delta \sim k_B T_K$ , can be calculated over a wide temperature range from the theory in question. If  $E_0$  is in the order of 100 to 200 meV, since  $S(\omega)$  is centered in a  $\Delta$  wide region, Eq. (4) becomes Eq. (3). Therefore, the decrease at high  $E_0$  of the curves in Fig. 4 is governed mainly by the decrease of  $F(\kappa)$  and not by that of  $S(\omega)$ , in agreement with the statements of (a). Using Eq. (4) the discrepancy at  $\vartheta = 8^\circ$ , visible in Fig. 6 can be explained by using an appropriate  $S(\omega)$ , i. e., an appropriate  $\Delta$ . The experimental results for the small momentum transfer region at any scattering angle should therefore be compared with Eq. (4).

The  $d\sigma_M/d\Omega$  values calculated from Eq. (4) for given  $T$  and  $\Delta$  values, utilizing a  $3d$ -type form factor for the Mn ion, are plotted with full lines in Fig. 4. The experimental data and calculated functions were mutually normalized in the vicinity of their maxima. From the theoretical curves fitted to the measured data we have  $\Delta = 30 \pm 5$  meV at room temperature, and  $\Delta = 50 \pm 5$  meV at  $80^\circ\text{K}$ . The temperature dependence of  $\Delta$  [from which  $\Delta_0 = \Delta(T=0)$ , and hence the Kondo temperature, can be determined] had a steeper slope in the temperature range under investigation than would follow from the classical formula of Nagaoka.<sup>4</sup>

From the experimental  $\Delta$  values it seems reasonable to take  $\Delta_0 = 60 \pm_{13}^{26}$  meV, which leads to a

Kondo temperature for  $AlMn$  of  $T_K = (700 \pm_{150}^{300})$  °K. This agrees well with the values obtained in other measurements.<sup>5,6</sup>

As seen in Fig. 4, the experimental and theoretical values of  $d\sigma_M/d\Omega$  display deviations, especially for small angles, if  $\kappa \rightarrow 0$ . For  $\kappa \rightarrow 1.1 \text{ \AA}^{-1}$ ,  $(d\sigma_M/d\Omega)_{\text{exp}} < (d\sigma_M/d\Omega)_{\text{theor}}$ , which is attributable to the change in the effective form factor. This discrepancy can be explained if a correlation length of  $\xi \sim 6 \text{ \AA}$  is supposed, in agreement with the results of other measurements.<sup>5</sup> Finally, a rapid increase of the measured data was observed for very small  $\kappa$  values, which could be ascribed to differences in the microstructure of the  $Al/Mn$  and  $Al$  samples.

To sum up, the comparison of a Kondo-type picture with the experimental  $d\sigma_M/d\Omega$  data permits the following conclusions.

(i) The high in-going energy cross section seems to be able to be described with the simple paramagnetic expression of (3), thus proving that the magnetic moment on the magnetic site is not zero.

(ii) At smaller ingoing energies (or  $\kappa$  values) two types of discrepancy occur. The first is connected with the presence of spin fluctuations. The spectrum of these fluctuations displays a maximum at an energy which depends on temperature. The position of this maximum, as can be deduced from the curves on Fig. 4, occurs at different  $\kappa$  values for different scattering angles, i. e. the anomaly is not characterized by a well-defined  $\kappa$  value. It is, however, characterized by a parameter  $\Delta$  which is the same for all scattering angles.

The other anomaly is connected with the discrepancy of the measured and calculated cross sections of Fig. 4, in which a  $3d$ -type form factor was assumed, and occurs at a well-defined  $\kappa$  value. It can therefore be attributed to the presence of a polarized electron cloud around the  $Mn$  atoms which fluctuates together with the magnetic moment of the impurity.

Considering that the evaluation of the measured data yielded very reasonable  $T_K$  and  $\xi$  values,

which are supported by other measurements, we conclude that the assumptions of Ref. 1 concerning the dynamic character of the  $s$ - $d$  exchange interaction are valid. At the same time, it can be regarded as indirect evidence of the inelastic nature of the diffuse paramagnetic scattering of neutrons in the range  $T \ll T_K$ .

Although the agreement with theory appears convincing, it should be mentioned that the integral character of our data leads to difficulties of interpretation. These can be avoided only if  $S(\omega)$  is measured directly via the  $d^2\sigma/d\Omega dE$  inelastic-scattering cross section.

It is known that the Kondo model gives a good description of alloys in the magnetic limit [in the Anderson notation  $U/\pi\Delta' \gg 1$  (Ref. 7)] as, e. g., of  $CuMn$ .  $AlMn$  does not differ fundamentally from this case although  $U/\pi\Delta' \sim 1$  and therefore it is not surprising that we obtained a good agreement with the theory based on this model.

It is important to stress that present experimental results give straightforward evidence as to the existence of a nonzero magnetic moment on  $Mn$  in  $AlMn$ . This moment is compensated at low temperatures by a polarized electron cloud. At high temperatures the magnetic character of the system is expected. Therefore, the spin-fluctuation picture, where no localized magnetic moment is supposed on the impurity site, does not describe the  $AlMn$  system.

The Rivier-Zuckerman<sup>8</sup> LSF picture is in good agreement with experiments in the nonmagnetic limit  $U/\pi\Delta' \ll 1$  and leads to similar qualitative results as those of the Kondo model when extrapolating for the  $U/\pi\Delta' \sim 1$  case, since both approximations are based on the Anderson model. The calculations for the LSF case are, however, much more complicated than for the Kondo type and therefore it is more difficult to get useful results.

Recently, the neutron scattering cross section for LSF systems has been calculated.<sup>9</sup> The qualitative picture of the scattering pattern is similar to that of the Kondo case.

\*On leave from Kossuth Lajos University, Debrecen, Hungary.

<sup>1</sup>G. E. Gurgenshvili, A. A. Nersesian, G. A. Haradze, Zh. Eksp. Teor. Fiz. **56**, 2028 (1968) [Sov. Phys. -JETP **29**, 1089 (1969)]; and the Phys. Inst. in Tbilisi 05-TT, 1972 (unpublished); and private communications.  
<sup>2</sup>C. Stassis and C. G. Shull, Phys. Rev. B **5**, 1040 (1972).  
<sup>3</sup>N. Kroó, Zs. Szentirmay, D. Jovic (unpublished). N. Kroó, Z. Szentirmay, Phys. Lett. A **40**, 173 (1972).  
<sup>4</sup>Y. Nagaoka, Phys. Rev. **138**, A1112 (1965); J. Phys. Chem. Solids **27**, 1139 (1966).

<sup>5</sup>N. Kroó, Zs. Szentirmay, *Proceedings of Twelfth International Conference on Low Temperature Physics*, edited by Eizo Kanda (Academic of Japan, Kyoto, 1971), p. 559.

<sup>6</sup>E. Kovács-Csetényi, F. Kedves, L. Gergely, G. Grüner, J. Phys. F **2**, 499 (1972).

<sup>7</sup>P. W. Anderson, Phys. Rev. **124**, 41 (1961).

<sup>8</sup>N. Rivier, M. Zuckerman, Phys. Rev. Lett. **21**, 904 (1968).

<sup>9</sup>K. Fischer (unpublished).